Contrast Ratio during Visualization of Subsurface Optical Inhomogeneities in Turbid Tissues: Perturbation Analysis

Gennadi Saiko[a] and Alexandre Douplik[b]
Department of Physics, Ryerson University, Toronto, Canada

Keywords: Biomedical Imaging, Diffuse Approximation, Turbid Tissues.

Abstract: Visualization and monitoring of the capillary loops and microvasculature patterns in dermis and mucosa are of interest for various clinical applications, including early cancer and shock detection. We developed an approach for the assessment of the contrast ratio during the visualization of subsurface optical heterogeneities. Using the diffuse approximation and perturbation analysis, we considered light absorption heterogeneities as negative light sources. We estimated the contrast ratio as a function of the surface layer's optical properties for diffuse and collimated wide beam illumination. Based on findings, we formulated several practical suggestions: a) proper selection of camera (with maximum dynamic range) is of paramount importance, b) narrow-band illumination is more efficient than white light illumination, and c) use of collimated light provides up to 60% improvement in contrast vs. diffuse illumination. Obtained results can be used for the optimization of imaging techniques

1 INTRODUCTION

Visualization and monitoring of capillary loops in the dermis and mucosa are of interest for various clinical applications, including early cancer and shock detection (Kanawade, 2010). Unusual capillary and capillary loop shapes can be precursors of cancer transformations (e.g., angiogenesis) or auto-immune diseases (scleroderma). Rapid changes in their shape and sizes can be one of the first signs of shock development. This interest drives continuous improvements in image quality in traditional optical systems and rapidly emerging lensless (Schelkanova, 2016) optical systems.

Because of the low-contrast nature of images of absorption patterns ("defects") in highly-light-scattering biotissues, several techniques were proposed to increase this contrast – (1) a narrow band imaging providing a better contrast than white light imaging (Saiko, 2020); (2) optical clearing to improve the imaging quality; (3) transformation and analysis of the image into a different colorspace (e.g., RGB->HSV) where subsurface inhomogeneity or "defect" appears enhanced (Zhanwu, 2006). In particular, Goffredo et al. (Goffredo, 2012) considered various color channel transformations to increase sensitivity and specificity for such defect discovery.

Given the continuous efforts to increase the superficial tissue image quality, it is essential to estimate its potential limitations. In our previous works, we have tried to evaluate the limits of defect detectability; namely a defect detectability depth (a maximum depth at which the defect can be detected) using computer simulations and a simple lattice model (Saiko, 2012). Initial assessment predicted (Saiko, 2012) that the detectability depth is limited by $1/\mu'_s$, where μ'_s is the reduced scattering coefficient of the surface layer. However, more rigorous analysis is required, which needs to include quantifiable parameters relevant, in particular, to human perception. A contrast ratio defined according to Weber's law as $c(x) = (I_b - I(x))/I_b$, where I_b and $I(x)$ is the intensity at the background and a point x, respectively, can serve as such parameter (Saiko, 2014a; Saiko, 2020)). We define a threshold contrast ratio, $c_{th,}$ as a minimum contrast ratio, which can be resolved by a particular optical device. Our definition implies that an optical system can not visualize the

[a] https://orcid.org/0000-0002-5697-7609
[b] https://orcid.org/0000-0001-9948-9472

Saiko, G. and Douplik, A.
Contrast Ratio during Visualization of Subsurface Optical Inhomogeneities in Turbid Tissues: Perturbation Analysis.
DOI: 10.5220/0010374100940102
In *Proceedings of the 14th International Joint Conference on Biomedical Engineering Systems and Technologies (BIOSTEC 2021) - Volume 2: BIOIMAGING*, pages 94-102
ISBN: 978-989-758-490-9

defect if the measured contrast ratio is less than c_{th}. Respectively, a detectability depth Z can be defined as a defect depth, where the measured contrast ratio for the defect is equal to c_{th}. Z is a function of a) the threshold contrast ratio, b) the optical tissue parameters (absorption coefficient, scattering coefficient, index of refraction, anisotropy factor), and c) defect parameters (volume, incremental absorption coefficient, and depth). Even though for a human eye, the threshold contrast ratio is around 0.1(Le, 2013), images with lower contrast ratio can be digitally enhanced and still can be used for feature examination or pattern recognition.

In automated processing scenarios, the threshold contrast ratio is limited by the camera's dynamic range, and we can estimate the threshold contrast ratio, which can be obtained using commercially available cameras. In the most typical scenario (e.g., with USB2 cameras), commercial cameras use 24bits for each pixel (3 colors x 8bits). A standard camera has 10-bit analog-to-digital converter (ADC), and due to bandwidth restriction in USB2 format, just 8 bits are employed. Thus, each channel's dynamic range is 2^8=256, making the camera facilitate the contrast ratio up to $c_{th\_\max} = \frac{1}{2^8 - 1} = 0.004$. A more realistic dynamic range (40%-80% of maximum) gives c_{th}=0.005-0.01. Similarly, for more advanced cameras (e.g., USB3 or GigE), each color channel is represented by 10-12bits, and the real dynamic range can be as high as 1600-3200, which consequently translates into c_{th}=0.0003-0.0006. In our assessments below, we will use c_{th}=0.01 and 0.001 as threshold contrast ratios, representing cameras with 8 and 12 bits per channel.

An analytical dependence of the contrast ratio on the depth of inhomogeneity location has been found (Dolin, 1997) for refractive index-matched boundary. In (Aksel, 2011), an absorber's depth was assessed using spatially resolved diffuse reflectance measurements. In the current work, we will evaluate how the depth of inhomogeneity location and optical parameters of the surrounding biotissue affect the image contrast in realistic conditions: a) refractive index mismatched boundary, and b) clinically relevant illumination scenarios (collimated and diffuse wide beam illumination). We will then use this information to find the detectability depth for such a defect for a particular optical system, which we will characterize using the threshold contrast ratio.

In a nutshell, we will determine the contrast ratio for a particular defect (defects), characterized by volume V and absorption coefficient $\delta\mu_a$, and located at the depth Z inside the tissue. Finding an exact solution to this problem in the general case is problematic. We will be looking for an approximate solution. For this purpose, we have developed a perturbation approach focusing on two typical illumination scenarios in biotissue imaging and spectroscopy (Saiko, 2014b): diffuse illumination (e.g., ambient light) and collimated wide beam illumination. To quantify the relative impact of each optical parameter on the detectability depth Z, we will determine dimensionless sensitivities (the relative change in the detectability depth Z for a given relative change in a parameter p, $(\Delta Z/Z)/(\Delta p/p)$) for all parameters (scattering or absorption coefficient, index of refraction, etc.).

2 METHODS

2.1 Tissue Model

Human skin and mucosal tissues have a layered structure (Meglinski, 2002). Based on our primary task to visualize the capillary grid, we can group covering tissues into (I) bloodless epithelium, (II) blood-containing papillary layer of the dermis (skin), or lamina propria (mucosa), and (III) underlying tissues (see Fig 1A). Living cells in epithelium receive oxygen and nutrients through the diffusion from capillaries located in the papillary layer underneath. Thus, the thickness of living cells epithelium layers is limited by the oxygen diffusion length and typically does not exceed 100μm. However, the stratum corneum, which includes "non-supplied" cells, can be much thicker in some organs, such as feet, soles, or palms.

2.2 Geometry

Based on our tissue model, the epithelium (including stratum corneum) can be considered an optical filter that covers absorption features and deteriorates the image's quality. To evaluate how the measured contrast ratio is affected by the presence of this outermost layer, we can consider the following model (see Fig 1B): the homogeneous top layer (Layer I) covers Layer II, which consists of 2 areas: a) homogeneous background, b) capillaries, which can be considered as heterogeneous (either absorption or scattering) features or "defects." Below this layer II, there is another layer III, which represents all underlying tissues. As we are interested in estimating the effects of the outermost surface layer, in order to simplify calculations, we can consider simplified geometry (Fig 1C): the homogeneous semi-infinite

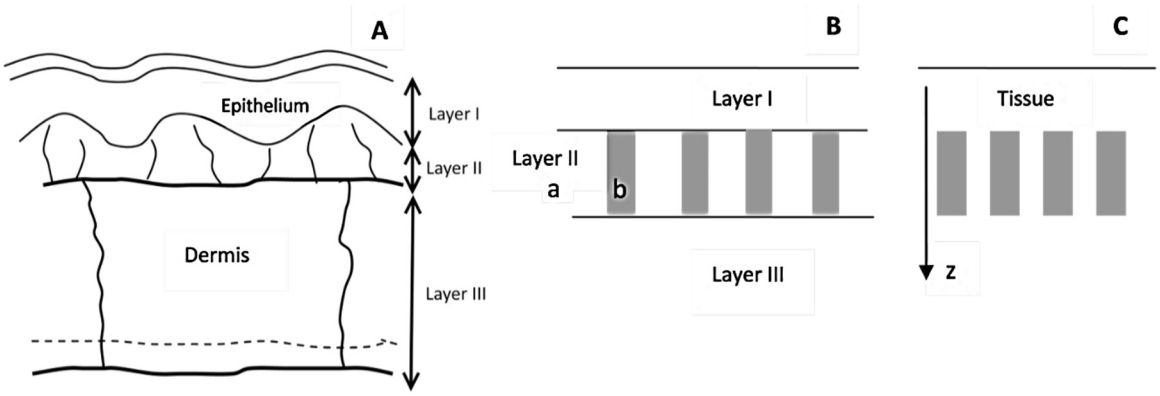

Figure 1: The logical transition from tissue microstructure (A) to heterogeneous dermis layer representation (B) to geometry that allows evaluating upper bound on the contrast ratio (C). Areas (a) and (b) of the panel B are background tissue and capillary (defect), respectively.

tissue characterized by an absorption coefficient μ_a and "defects" described by the volume V and absorption coefficient $\mu_a+\delta\mu_a$ and located at the depth Z (here $\delta\mu_a$ is an incremental absorption coefficient associated with the defect). In this case, the contrast presented by the features will be maximized, and we can estimate the upper bound (the best-case scenario) for visualization of these particular features.

2.3 Mathematical Model

The light propagation problem in homogeneous tissue can be solved exactly for specific geometries (e.g., slab, semi-space, or spheroid in diffuse approximation, slab and semi-space in Kubelka-Munk model (see, e.g. (Saiko, 2014b)). The presence of an arbitrary defect complicates things significantly, and we have to look for an approximate solution. A perturbation theory can be a useful approach to find such an approximate solution: we start from the exact solution for the semi-space geometry and add the defect as a perturbation. Our perturbation approach consists of the following steps:

1. We find a solution for light distribution in homogeneous semi-infinite tissue (the radiant energy fluence rate $\varphi(\vec{r})$ (W/m^2)).

2. If we know the radiant energy fluence rate $\varphi(\vec{r})$ at some particular point $\vec{r}$, then we can calculate additional (or incremental) absorbed optical power density $\delta\mu_a\varphi(\vec{r})$ (W/m^3) for some optical heterogeneity with the absorption coefficient $\mu_a+\delta\mu_a$ located at this point. If the volume of the heterogeneity is V, then the additional power absorbed at this heterogeneity will be $\delta\mu_a\varphi(\vec{r})V$ (W).

3. Alternatively, the heterogeneity can be considered a negative (or inverse) point source with power $-\delta\mu_a\varphi(\vec{r})V$, located at the point $\vec{r}$. The radiant energy fluence rate induced by such a source can be calculated exactly.

This problem can be analyzed using the diffuse approximation (Star, 2011).

Step 1: For a semi-infinite medium with wide beam diffuse illumination, the total radiant energy fluence rate within the tissue far from the borders of the beam depends only on the depth z (Eq. 6.88 in (Star, 2012)):

$$\varphi_d(z)=\frac{4}{1-r_{21}}\frac{\exp(-\mu_{eff}z)}{1+h\mu_{eff}} \quad (1)$$

Where $\mu_{eff}=\sqrt{\mu_a/D}$, $D=1/3\mu_{tr}$, $\mu_{tr}=\mu_a+\mu_s(1-g)$, r_{21} is the coefficient of reflection of diffuse light on the border of tissue and air (r_{21} can be approximated using the relative index of refraction n: $r_{21}\approx 1-n^{-2}$), $h=2D\frac{1+r_{21}}{1-r_{21}}$. Here without losing generality (we are looking for the contrast ratio, which is dimensionless), we also assumed that the incident light's surface density is 1 (W/m2).

Similarly, we can solve the semi-infinite problem for wide beam collimated illumination. The difference here is the presence of collimated term, which dissipates proportionally to $\exp(-(\mu_a+\mu_s)z)$. For the biologically relevant

case, $\mu_a << \mu_s$ we have an expression (Eq. 6.83 in (Star, 2012)):

$$\varphi_c(z) = \frac{5-r_{21}}{1-r_{21}} \frac{\exp(-\mu_{eff} z)}{1+h\mu_{eff}} - 2\exp(-(\mu_a+\mu_s)z) \quad (2)$$

The advantage of the wide beam diffuse illumination scenario is that it allows obtaining closed-form expressions. We omit collimated light calculations for the sake of brevity and present only results.

Step 2: The additional power absorbed at the inhomogeneity can be found by multiplication of Eq.1 or 2 on $V\delta\mu_a$,

Step 3: The diffuse source with power P in isotropic medium generates radiant energy fluence rate on the distance R from the source

$$\varphi_s(R) = \frac{3P\mu_{tr}}{4\pi R}\exp(-\mu_{eff} R) \quad (3)$$

Thus, we can represent our defect as the point source described by Eq.3, where power P is the power calculated on step 2 with a minus sign (negative source). To take into account the boundary conditions, we can use the diffusion dipole model (Frerrerd, 1973; Kienle, 1994). In addition to the initial source located at depth Z, we can consider the second source (with opposite sign) located on the distance $2h+Z$ above the surface. In this case, total flux approximately satisfies realistic boundary condition for all r ($r = \sqrt{x^2+y^2}$) and z=0 (Haskell, 1994)

$$\varphi(r,z) - h\frac{\partial\varphi(r,z)}{\partial z} = 0 \quad (4)$$

3 RESULTS

If the inhomogeneity is located at *(0,0,Z)*, then the fluence rate at any point on the surface of the tissue surface (here we assume cylindrical coordinates) in the presence of mismatched border will be:

$$\varphi_s(r) = \frac{-3\delta\mu_a\varphi(Z)V\mu_{tr}}{4\pi} \times \left[\frac{\exp(-\mu_{eff}(Z^2+r^2)^{1/2})}{(Z^2+r^2)^{1/2}} - \frac{\exp(-\mu_{eff}((2h+Z)^2+r^2)^{1/2})}{((2h+Z)^2+r^2)^{1/2}}\right] \quad (5)$$

Where $\varphi(Z)=\varphi_d(Z)$ for diffuse illumination (Eq.1) and $\varphi(Z)=\varphi_c(Z)$ for collimated illumination (Eq.2).

Another realistic clinical scenario is to resolve two heterogeneities located under the surface using imaging techniques. It can be the case for assessing whether an imaging technique can visualize each blood capillary separately. Thus, we will consider two geometries: a single defect or heterogeneity (Fig. 2A) and two identical defects on the same depth (Fig. 2B).

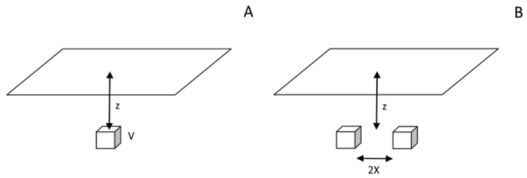

Figure 2: Geometry of heterogeneities: a single defect (A) and two defects (B).

3.1 Contrast in Case of a Single Heterogeneity

Let's consider a single inhomogeneity located at *(0,0,Z)* (see Fig 2A). Far from the inhomogeneity, its effect is negligible. Thus, we can take the unperturbed flux rate on the surface at this point as a background *($\varphi_b=\varphi(0)$)*. Near the inhomogeneity, we cannot ignore the flux rate from the inhomogeneity, $\varphi_s(r)$. If we compare the background flux with the fluence rate on the surface in the presence of the inhomogeneity *($\varphi(r)=\varphi(0)+\varphi_s(r)$)*, we can calculate the contrast ratio at any point on the surface of the tissue

$$c(r) = \frac{\varphi_b - \varphi(r)}{\varphi_b} = -\frac{\varphi_s(r)}{\varphi(0)} \quad (6)$$

here again $\varphi(0)=\varphi_d(0)$ for diffuse illumination (Eq.1) and $\varphi(0)=\varphi_c(0)$ for collimated illumination (Eq.2).

3.1.1 Diffuse Illumination

For diffuse illumination from Eq.5 with $\varphi(Z)=\varphi_d(Z)$ and Eq.6, we will get:

$$c(r) = \frac{3\mu_{tr}\delta\mu_a V\exp(-\mu_{eff}Z)}{4\pi} \times \left[\frac{\exp(-\mu_{eff}(Z^2+r^2)^{1/2})}{(Z^2+r^2)^{1/2}} - \frac{\exp(-\mu_{eff}((2h+Z)^2+r^2)^{1/2})}{((2h+Z)^2+r^2)^{1/2}}\right] \quad (7)$$

Immediately above the heterogeneity (r=0) from Eq.7, we can get a compact expression

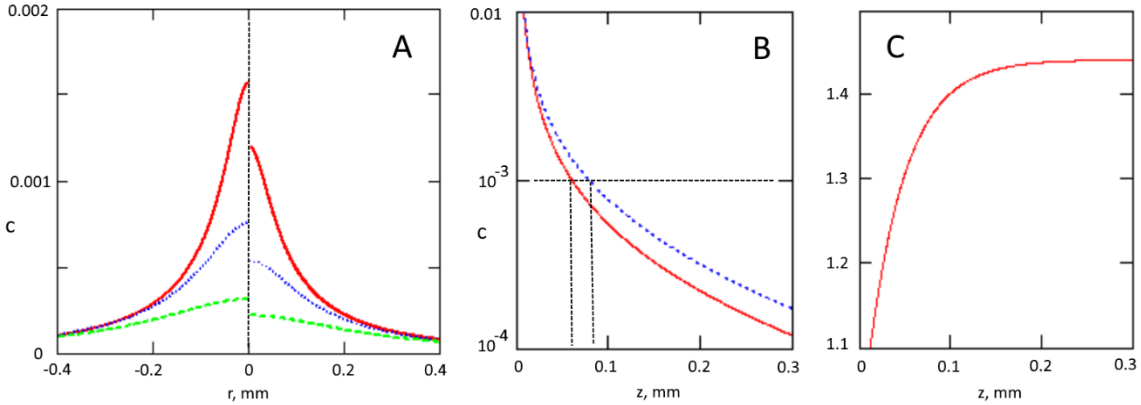

Figure 3: Panel A- radial dependence of the contrast ratio (collimated illumination- left side, diffuse illumination –right side) on the surface above the defect located at depth 0.05mm (solid red line), 0.1mm (dotted blue line) and 0.2mm (dashed green line). Panel B- the contrast in the point above the defect *c(0)* as a function of the defect depth (in mm) for wide beam diffuse (solid red line) and collimated (dotted blue line) illumination. Panel C- the ratio of contrasts for collimated illumination and diffuse illumination. Tissue parameters were: μ_a=0.033mm^{-1} and μ'_s=5mm^{-1} (reticular dermis), $\delta\mu_a$=28mm^{-1} (the whole blood with 70% oxygenation at 532nm), V=20x20x20μm^3, n=1.33.

$$c(0)=\frac{3\mu_{tr}\delta\mu_a V\exp(-2\mu_{eff}Z)}{4\pi}\times \left[\frac{1}{Z}-\frac{\exp(-\mu_{eff}2h)}{2h+Z}\right] \quad (8)$$

3.1.2 Collimated Illumination

We can also analyze how the contrast will be different for the same defect for diffuse and collimated illumination. As we just discussed, the contrast at any point on the surface of the tissue for the defect located on the depth Z taking into account Eq.6 would be $c(r)=-\varphi_s(r)/\varphi(0)$, here $\varphi(z)$ is the unperturbed flux distribution for either diffuse light (Eq.1) or collimated light (Eq.2). Thus, taking into account that for our negative source $\varphi_s(r)\sim-\delta\mu_a V\varphi(Z)\sim\varphi(Z)$ after simple reducing, we can find that the ratio of contrasts for collimated light and diffuse light will be

$$c_c/c_d=\frac{\varphi_c(Z)/\varphi_c(0)}{\varphi_d(Z)/\varphi_d(0)}= \frac{a}{a-2}-\frac{2}{a-2}\exp(-(\mu_a+\mu_s-\mu_{eff})z) \quad (9)$$

here for the sake of brevity, we introduced

$$a=\frac{5-r_{21}}{1-r_{21}}\frac{1}{1+h\mu_{eff}}.$$

We have analyzed the problem in a realistic case of the upper part of the capillary loop in the dermis:μ_a=0.033mm^{-1} and μ'_s=5mm^{-1} for reticular dermis (Meglinski, 2002), $\delta\mu_a$=28mm^{-1} (the whole blood with 70% oxygenation at 532nm), V=20x20x20μm^3, n=1.33. Results are presented in Fig 3.

Fig 3B shows that such defects can be visualized (with c_{th}=0.001) till approximately 0.07 mm for diffuse illumination and 0.09 mm for collimated illumination.

3.2 Contrast in Case of Double Heterogeneity

To analyze this problem for diffuse illumination, let's consider two heterogeneities located at *(X,0,Z)* and *(-X,0,Z)* (see Fig 2B). If we compare fluence rate on the surface far from the heterogeneities (background, $\varphi_b=\varphi_d(0)$) and the fluence rate on the surface in the presence of the inhomogeneities $(\varphi(x,y)=\varphi_d(0)+\varphi_s(x,y))$ we can calculate contrast ratio at any point *(x,y,0)* on the surface of the tissue. Using Eq. 5 for each inhomogeneity, we can get Eq. 10.

To distinguish these two heterogeneities, there should be some contrast between a point above any of these heterogeneities (e.g. *(X,0,0)*) and the point between two heterogeneities *(0,0,0)*- see Eq.11

So, if $\Delta c>c_{th}$, then we can distinguish two heterogeneities. In the opposite case, we will see them as a single heterogeneity with the length *2X*.

$$c(x,y)=\frac{\varphi_b-\varphi(x,y)}{\varphi_b}=\frac{3\mu_{tr}\delta\mu_a V\exp(-\mu_{eff}Z)}{4\pi}\times$$
$$\left[\frac{\exp(-\mu_{eff}(Z^2+(x-X)^2+y^2)^{1/2})}{(Z^2+(x-X)^2+y^2)^{1/2}}+\frac{\exp(-\mu_{eff}(Z^2+(x+X)^2+y^2)^{1/2})}{(Z^2+(x+X)^2+y^2)^{1/2}}-\right. \tag{10}$$
$$\left.-\frac{\exp(-\mu_{eff}((2h+Z)^2+(x-X)^2+y^2)^{1/2})}{((2h+Z)^2+(x-X)^2+y^2)^{1/2}}-\frac{\exp(-\mu_{eff}((2h+Z)^2+(x+X)^2+y^2)^{1/2})}{((2h+Z)^2+(x+X)^2+y^2)^{1/2}}\right]$$

$$\Delta c=c(X,0)-c(0,0)=\frac{3\mu_{tr}\delta\mu_a V\exp(-\mu_{eff}Z)}{4\pi}\times\left[\frac{\exp(-\mu_{eff}Z)}{Z}+\right.$$
$$+\frac{\exp(-\mu_{eff}(Z^2+4X^2)^{1/2})}{(Z^2+4X^2)^{1/2}}-\frac{\exp(-\mu_{eff}(2h+Z))}{2h+Z}-\frac{\exp(-\mu_{eff}((2h+Z)^2+4X^2)^{1/2})}{((2h+Z)^2+4X^2)^{1/2}}- \tag{11}$$
$$\left.-2\frac{\exp(-\mu_{eff}(Z^2+X^2)^{1/2})}{(Z^2+X^2)^{1/2}}+2\frac{\exp(-\mu_{eff}((2h+Z)^2+X^2)^{1/2})}{((2h+Z)^2+X^2)^{1/2}}\right]$$

We have analyzed the problem in a realistic case of upper part of capillary loop in dermis: μ_a=0.033mm^{-1} and μ'_s=5mm^{-1}, $\delta\mu_a$=28mm^{-1}, V=20x20x20μm^3, n=1.33, X=0.1mm. Results are presented in Fig 4.

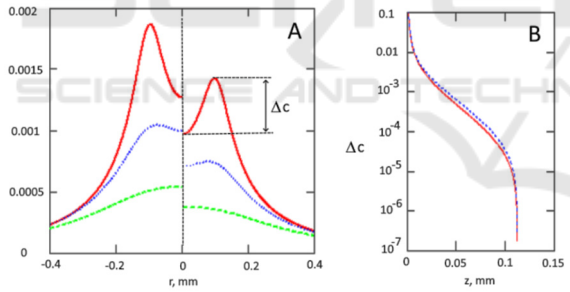

Figure 4: Panel A- Dependence of the contrast ratio (collimated illumination – left side, diffuse illumination- right side) on the surface above the defects located at depth 0.05mm (solid red line), 0.1mm (dotted blue line) and 0.2mm (dashed green line). Panel B- Δc(difference in contrast in the point above the defect c(X,0) and between defects c(0,0)) as a function of the defect depth Z (in mm) for wide beam diffuse (solid red line) and collimated (dotted blue line) illumination. Tissue parameters: μ_a=0.033mm^{-1}, μ'_s=5mm^{-1}, $\delta\mu_a$=28mm^{-1} (the whole blood with 70% oxygenation at 532nm), V=20x20x20μm^3, n=1.33. Half distance between defects X=0.1mm.

Resolution depth for such scenario is approximately 0.034mm (for c_{th}=0.001).

In addition, we have calculated the sensitivity of observables (detectability depth and contrast ratio) to changes in any optical tissue parameters (Δz/z/Δp/p, where p is an optical tissue parameter, e.g., absorption coefficient) by varying each optical parameter (μ_a, $\delta\mu_a$, V, n) and half-distance between defects X by -20%, -10%, 10%, and 20%. We also split μ'_s into μ_s and g and studied each of these variables separately (assuming g=0.8, μ_s =25mm^{-1}). Results for the normal skin (Meglinski, 2002) are presented in Table 1.

For example, one can see that in the case of a single defect imaged with an 8-bit camera (c_{th}=0.01), the largest relative impact has the anisotropy factor: 1% change in the anisotropy factor leads to a 3.6% change in the detectability depth. In this case, the effect can be ranked (from the highest to the lowest): the anisotropy factor, defect parameters ($\delta\mu_a$, V), scattering coefficient, index of refraction. The impact of the absorption coefficient of the tissue is relatively minimal.

Table 1: Dimensionless sensitivities ((Δz/z)/(Δp/p)) of observables (in rows) to changes in optical parameters of the tissue (μ_a, μ_s, g, n) and defect ($\delta\mu_a$, V, X).

Observables	μ_a	μ_s	g	n	X	$\delta\mu_a$V
Detectability depth z for c_{th}=0.01 (single defect)	0.00	0.90	-3.60	0.10	n/a	0.90
Detectability depth z for c_{th}=0.001 (single defect)	-0.06	0.51	-2.15	0.41	n/a	0.72
Detectability depth z for c_{th}=0.01 (double defect)	0.00	0.79	-2.89	0.00	0.26	0.79
Detectability depth z for c_{th}=0.001 (double defect)	0.00	0.32	-1.43	0.00	0.67	2.59
Contrast ratio c for the defect located at z=0.1mm	-0.06	0.76	-3.25	0.76	n/a	1.08

4 DISCUSSION AND CONCLUSIONS

We have analyzed several scenarios that can be used for image quality characterization in tissue imaging. We found that various optical parameters contribute differently to the contrast ratio. The absorption coefficient of the tissue does have a very minimal impact. The most substantial effect has the anisotropy factor g (due to our initial value g=0.8, it is approximately four times $(g/(1-g))$ stronger than μ_s), followed by properties of the defect and scattering coefficient of the tissue. The refraction index and the distance between defects have minimal impact. These data provide the relative impact of various factors on the experiment's accuracy and can be used to guide experimental and Monte Carlo simulations.

While a few tissue optical parameters can be varied in an experiment (e.g., tissue scattering coefficient and refraction index through optical clearing), the absorption coefficient for inhomogeneity is the single factor that can be varied in practice. Moreover, the contrast linearly depends on this factor, and detection depth strongly depends on it as well (high sensitivity, see Table 1). Thus, proper wavelength selection (e.g., at the absorption peak of hemoglobin) is of paramount importance for visualization.

We considered two realistic illumination scenarios: wide beam diffuse illumination (e.g., ambient light) and wide beam collimated illumination (e.g., a medical light source, laser). Results are very similar. However, it should be noted that collimated illumination provides better image contrast (see Fig 3B and 4B for comparison). For our parameters, 40% contrast improvement can be achieved using collimated illumination (see Fig 3C). We can estimate the maximum enhancement provided by the collimated light. Taking into account that $\mu_s >> \mu_a, \mu_{eff}$ and using Eq.9, we can find that for deep defects ($Z >> 1/\mu_s$)

$$c_c / c_d \to \frac{a}{a-2} = \frac{5-r_{21}}{5-r_{21}-2(1-r_{21})(1+h\mu_{eff})} \quad (12)$$

In case of the matched boundary ($r_{21} = 0$):

$$c_c / c_d \to 5/(3-4\sqrt{\mu_a / 3\mu_{tr}}) \quad (13)$$

Such as in most tissues $\mu_s >> \mu_a$, this ratio can be estimated as 5/3. That means that for the matched boundary, collimated light provides 66% improvement over diffuse light. These results are in agreement with previously reported models (Saiko, 2020).

If we know the contrast ratio associated with the defect, we can assess whether a particular imaging system can visualize it. Namely, if the camera's threshold contrast ratio is above the defect contrast ratio, the defect can be imaged. We assessed that the realistic threshold contrast ratio for commercially available cameras is in the 0.01-0.001 range for 8-12 bits cameras. Because the dynamic range of a camera used in measurements is the primary factor limiting the recognition of objects with low contrast, the proper selection of a camera is vital for imaging subsurface structures.

Out estimations of the defect detectability depth are in a qualitative agreement with MC simulations (Saiko, 2014a). In particular, MC simulations have shown (Saiko, 2014a) that diffuse reflectance spectroscopy can potentially identify absorption inhomogeneities located at a depth of 0.5–1.0 of the transport mean free path $l_s = 1/\mu_s'$.

It should be noted that the proposed "detectability depth" is different from a mean sampling (or interrogation) depth (see, e.g. (Bevilacqua, 2004)). The mean sampling depth can be viewed as the first moment of the photon scattering density function (or PSDF) for various photon trajectories (e.g., in a Monte Carlo simulation). The mean sampling depth depends on the tissue's optical properties (μ_a and μ_s') and source-detector separation (if any). The detectability depth depends on μ_a and μ_s', the properties of the defect (namely volume V and absorption coefficient $\delta\mu_a$), and the imaging system's properties (namely the threshold contrast ratio c_{th}).

Conceptually, our approach is a perturbation expansion. The zeroth term is the light distribution in a homogeneous semi-infinite issue, and the first-order term is the linear contribution caused by the presence of inhomogeneities (defects).

To keep the perturbation approach valid, we need to satisfy several conditions. Firstly, the light field change within the defect caused by its absorption properties should be small. Given that the defect in our case is illuminated from all sides, then the impact will be negligible if $\delta\mu_a V^{1/3} / 2 << 1$, which is satisfied for our defect parameters.

Secondly, the diffuse approximation provides accurate light distribution far from sources and borders: when the mean optical free path ($1/\mu_t$) is much smaller than the size under consideration. For our quasi-1D problem, the defect depth z is the only characteristic size and $\mu_t z \approx 1$. However, the diffuse approximation is still a useful approximation, even

close to boundaries (Chai, 2008). In particular, (Lehtikangas, 2012) found that the relative error of fluence rate near the surface is between 3.73% and 6.31% for the DA when μ_s = 50 mm^{-1} and μ_s = 5 mm^{-1}, respectively. Such as we intend to provide rough estimations (e.g., feasibility assessment of technology, estimate maximum detectability depth for a particular wavelength, select appropriate bit depth for the camera), we expect that its major conclusions will hold.

In addition to general questions about the applicability of the diffuse approximation, some additional questions arise while using this perturbation approach: a) what is the volume of the heterogeneity to keep this approach valid, and b) if we have multiple heterogeneities, what are the criteria to make sure that they do not interact with each other, namely that their impacts are additive.

To address the first question, we can consider that we have a one-dimensional problem with constant illumination in the horizontal plane in the zeroth approximation. Thus, the defect will be small enough if the light distribution within the defect will be homogeneous: $\partial\varphi/\partial z\, l_z << \varphi$, where l_z is the vertical size (the height on Fig 2A) of the defect. Taking into account Eq.1, this condition can be rewritten as $\mu_{eff} l_z << 1$.

The requirement (b) can be reformulated as follows: the fluence rate induced by all other defects is much smaller than the homogeneous field at this point. Using Eq.1 and Eq.2, we can estimate the required distance R between defects with volume V as: $R_0 = \frac{3\delta\mu_a V \mu_{tr}}{4\pi} << R$, which is less than 1μm for our parameters.

In light of requirement (b), we can take a look at the applicability of our approach to vertical (e.g., capillaries) and horizontal (e.g., nail fold capillaries) linear heterogeneities. One can easily find that due to slow descendants of the fluence rate induced by a single defect (Eq.3), the integral of the fluence rate diverges at any point of the continuous curve of sources. Thus, even though it is possible to calculate the impact of inhomogeneity in these scenarios, such solutions' validity will be doubtful. Consequently, this approach can be applied only to sets of discrete heterogeneities with distances between them $R >> R_0 = \frac{3\delta\mu_a V \mu_{tr}}{4\pi}$.

If the inhomogeneity's parameters are known (e.g., in the case of a blood vessel), then the contrast ratio can be used to extract the surface layer's parameters, e.g., its thickness. Measuring contrast at multiple wavelengths (e.g., multispectral or hyperspectral imaging) may obtain further insights into the epithelial layer's composition.

As a natural extension of previous works (Saiko, 2012, 2014a, 2014b), the current results explicitly contain absorption coefficient, thus allowing a direct MC verification.

In summary, we propose a simple perturbation model, which links optical tissue parameters with the contrast ratio in reflectance imaging geometry. Using the proposed model, we derived explicit expressions for the contrast ratio in the case of tissue imaging with diffuse and collimated wide beam illumination. Using the contrast ratio, the detectability depth can be estimated for a particular imaging system. The relative impact of optical tissue parameters on the detectability depth can also be determined. The proposed approach can be exploited for the assessment and optimization of tissue imaging techniques.

ACKNOWLEDGEMENTS

The authors would like to acknowledge the support for this study from NSERC Discovery grant (Douplik), Ryerson Health Fund, NSERC Engage support, and infrastructural support from Institute for Biomedical Engineering, Science and Technology (IBEST), a partnership between Ryerson University and St. Michael's Hospital (Toronto).

REFERENCES

Kanawade, R. et al., 2010, Vessel density modulation detection in skin model by using spatially resolved diffuse reflectance techniques for application of early sign of shock detection. *Photodiagnosis and Photodynamic Therapy*; 7: P14

Schelkanova, I. et al., 2016, Spatially resolved, diffuse reflectance imaging for subsurface pattern visualization toward development of a lensless imaging platform: phantom experiments. *J. Biomed. Opt*.21 (1): 015004.

Saiko, G., Betlen, A., 2020, Optimization of Band Selection in Multispectral and Narrow-Band Imaging: an Analytical Approach, *Adv. Exp Med Biol* 1232:361-367.

Zhanwu, X., Miaoliang, Z., 2006, Color-based skin detection: survey and evaluation. In: Proceedings of the *12th International Conference on Multi-Media Modelling*, vol 10, Beijing.

Goffredo, M. et al., 2012, Quantitative color analysis for capillaroscopy image segmentation, *Med Biol Eng Comput* 50:567–574

Saiko, G. Douplik, A., 2012, Real-Time optical monitoring of capillary grid spatial pattern in epithelium by spatially resolved diffuse reflectance probe, *J Innov. Opt. Heal. Scie*., 05(02): 1250005

Saiko G. et al., 2014 Optical Detection of a Capillary Grid Spatial Pattern in Epithelium by Spatially Resolved Diffuse Reflectance Probe: Monte Carlo Verification, *Sel. Top. Quantum Electron. IEEE J*. 20(2): 7000609

Le D. et al., 2013, Monte Carlo modeling of light–tissue interactions in narrow band imaging, *J. Biomed. Opt*., 18 (1): 010504-1–010504-3.

Dolin, L.S., 1997 On the possibility of detecting an absorbing object in a strongly scattering medium using the method of continuous optical sounding, *Radiophysics and Quantum Electr*, 40(10): 799-812.

Aksel, E.B., et al., 2011, Localization of an absorber in a turbid semi-infinite medium by spatially resolved continuous-wave diffuse reflectance measurements. *J Biomed Opt*.; 16(8):086010.

Saiko, G. Douplik, A., 2014, Reflectance of Biological Turbid Tissues under Wide Area Illumination: Single Backward Scattering Approach*, Int. J. of Photoenergy*, 241364

Meglinski, I. V. Matcher, S. J., 2002, Quantitative assessment of skin layers absorption and skin reflectance spectra simulation in the visible and near-infrared spectral regions, *Physiol. Meas*. 23:741753.

Star, W.M., 2011, Diffusion Theory of Light Transport, in *Optical-Thermal Response of Laser-Irradiated Tissue* (2nd Ed) Ed. by A.J. Welch, Dordrech, NLD: Springer,

Frerrerd, R.J. Longini, R.L. 1973, Diffusion dipole source, *J. Opt. Soc. Am*. 63: 336-337

Kienle, A., Patterson, M.S, 1994, Improved solutions of the steady-state and the time-resolved diffusion equations for reflectance from a semi-infinite turbid medium, *J. Opt. Soc. Am*. A 14: 246-254.

Haskell R.C., et al., 1994, Boundary conditions for the diffuse equation in radiative transfer, *J. Opt. Soc. Am*. A 11: 2727-2741.

Bevilacqua F. et al., 2004, Sampling tissue volumes using frequency-domain photon migration. *Phys. Rev. E*; 69(5):51908.

Chai, C. et al. 2008, Analytical solution of P3 approximation to radiative transfer equation for an infinite homogenous media and its validity, *J. Modern Opt*, 55(21): 3611-3624.

Lehtikangas, O. et al., 2012, Modeling boundary measurements of scattered light using the corrected diffusion approximation. *Bio Opt Exp*. 3(3):552–571.